Ferromagnetism

DOI: 10.1002/anie.201309416

Unexpected Room-Temperature Ferromagnetism in Nanostructured Bi_2Te_3**

Guanjun Xiao, Chunye Zhu, Yanming Ma, Bingbing Liu, Guangtian Zou, and Bo Zou**

Abstract: *There is an urgent need for the development in the field of the magnetism of topological insulators, owing to the necessity for the realization of the quantum anomalous Hall effect. Herein, we discuss experimentally fabricated nanostructured hierarchical architectures of the topological insulator Bi_2Te_3 without the introduction of any exotic magnetic dopants, in which intriguing room-temperature ferromagnetism was identified. First-principles calculations demonstrated that the intrinsic point defect with respect to the antisite Te site is responsible for the creation of a magnetic moment. Such a mechanism, which is different from that of a vacancy defect, provides new insights into the origins of magnetism. Our findings may pave the way for developing future Bi_2Te_3-based dissipationless spintronics and fault-tolerant quantum computation.*

Bismuth telluride (Bi_2Te_3) has long been known as one of the best thermoelectric materials, and for its transformation into superconducting states under high pressure.[1] Recent studies demonstrate that the magnetoresistance switching effect and a weak localization bulk state can be achieved experimentally in Bi_2Te_3-based materials, which makes them highly attractive for future novel magnetoelectronic device applications.[2] In particular, the latest discovery of Bi_2Te_3 as the simplest three-dimensional topological insulator with a single Dirac cone on the surface makes it even more fascinating.[3] When magnetic elements (such as Cr or Fe) are introduced into the Bi_2Te_3 family of topological insulators, the quantum anomalous Hall (QAH) effect can be realized, associated with the breaking of time-reversal symmetry induced by magnetic ordering.[4] Moreover, Bi_2Te_3 is anticipated to serve as a platform for novel Majorana fermions and image magnetic monopole harvesting once magnetism is introduced.[5]

Thus far, the creation of magnetism in topological insulators has largely relied upon the introduction of external magnetic elements. As a result, the magnetism generated is extrinsic, and possibly presents difficulties for the industrial fabrication of electronic devices. Herein, we report the experimental fabrication of magnetically nanostructured hierarchical architectures (HAs) of Bi_2Te_3 without introducing any exotic magnetic dopants. This was accomplished through a simple, but highly adaptable, solution-phase strategy. Also, an intriguing room-temperature ferromagnetism (RTFM) was identified in the product. First-principles calculations demonstrate that the intrinsic point defect with respect to the antisite Te site is responsible for the creation of a magnetic moment. Such a mechanism, which is different from that of a vacancy defect, provides new insights into the origins of magnetism. Our findings provide the possibility to create intrinsic ferromagnetism in topological insulators, thus paving the way for developing future Bi_2Te_3-based dissipationless spintronics and fault-tolerant quantum computing.

Figure 1 a,b shows the typical field emission scanning electron microscopy images of the sample at low and high magnifications. We can clearly see that the as-prepared products possess caterpillar-like HAs with dimensions up to the micrometer scale. Chemical composition of the obtained

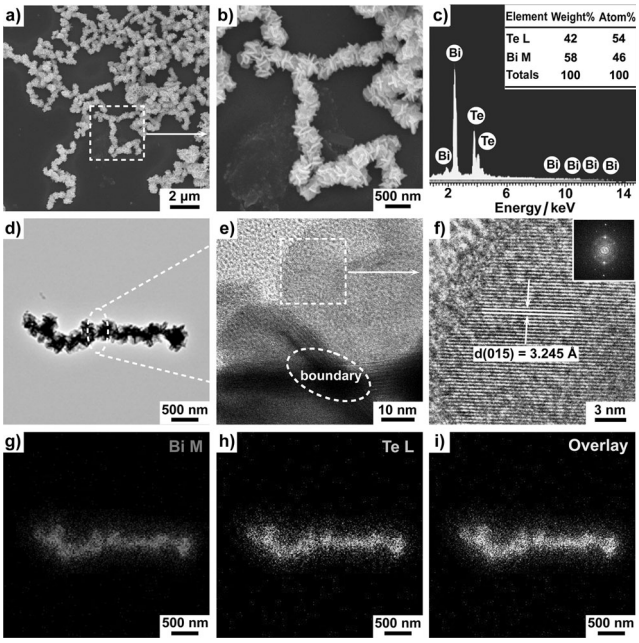

Figure 1. Morphology and structure of as-prepared nanostructured Bi_2Te_3 HAs. a,b) FESEM images at different magnifications. c) EDX analysis of Bi-rich Bi_2Te_3. d,f) TEM and HRTEM images of the obtained Bi_2Te_3 HAs. The inset in (f) shows the corresponding fast Fourier transform pattern. g–i) Element-distribution mapping showing the distribution of Bi and Te.

[*] Dr. G. Xiao,[+] Dr. C. Zhu,[+] Prof. Y. Ma, Prof. B. Liu, Prof. G. Zou, Prof. B. Zou
State Key Laboratory of Superhard Materials, Jilin University
Changchun 130012, (P. R. China)
E-mail: zoubo@jlu.edu.cn
mym@jlu.edu.cn

[+] These authors contributed equally to this work.

[**] We gratefully acknowledge funding support from the National Natural Science Foundation of China (91227202, 11025418, and 91022029), RFDP (20120061130006), and the National Basic Research Program of China (2011CB808200).

Supporting information for this article is available on the WWW under http://dx.doi.org/10.1002/anie.201309416.

products was examined by energy-dispersive X-ray analysis. The stoichiometric ratio of Bi/Te is about 2:3, with a slight Bi enrichment (Bi: 46%, Te: 54%; Figure 1c). The transmission electron microscopy (TEM) image further reveals a caterpillar-like morphology with a HAs length of about 2 μm (Figure 1d). High-resolution TEM images present apparent boundaries and continuous lattice fringes, which are indicative of the crystalline-like nature (Figure 1e,f). Moreover, interplanar spacing was measured to be about 3.245 Å, which corresponds to the (015) facet of the rhombohedral phase of Bi_2Te_3 (Figure 1f). Elemental distribution maps indicate that the elements of Bi and Te are homogeneously distributed throughout the whole sample, which suggests a high purity of the final products (Figure 1g–i). Furthermore, we carried out Rietveld refinements of the X-ray diffraction pattern (Supporting Information, Figure S1) which dovetail well into the rhombohedral phase Bi_2Te_3, with a space group of $D^5{}_3d$ ($R\bar{3}m$) and $R_{wp} = 11.06\%$ and $R_p = 8.46\%$. Also, no peaks of other elements except C, O, Bi, and Te are observed in the X-ray photoelectron spectroscopy images (Figure S2), which further indicates the high purity of the products.

Owing to their unique structures, HAs are anticipated to offer new opportunities in diverse fields.[6] As for our present study, it is exciting that the prepared caterpillar-like Bi_2Te_3 HAs exhibit RTFM behavior, as measured with a Quantum Design SQUID magnetometer. Figure 2a represents the typical magnetic performance of the samples in magnetic fields of up to ±30 kOe at temperatures of 5 and 300 K. It can be clearly seen that the hysteresis loop at 5 K shows no magnetic saturation, even as the magnetic field reaches the maximum. At 300 K, although the ferromagnetism has been suppressed, it apparently persists with a saturated magnetization at 0.017 emu g^{-1}. The inset in Figure 2a shows a visible coercivity decreasing from 110 Oe at 5 K down to 40 Oe at 300 K. Figure 2b depicts the temperature-dependent magnetizations of the Bi_2Te_3 HAs samples within field-cooled (FC) and zero-field-cooled (ZFC) procedures under an applied field of 500 Oe. The ZFC magnetization increases gradually up to approximate 170 K, and then declines slowly, suggesting that the blocking temperature (T_B) is 170 K. This up and down behavior in the ZFC curve is understandable. As the temperature increases up to T_B, the thermal energy disturbs the system and more moments acquire the energy to be aligned with the external field direction. Above T_B, the thermal energy is strong enough to randomize the magnetic moments, thus leading to a decrease in magnetization. Moreover, the FC and ZFC plots exhibit distinct bifurcation at the onset near 350 K (Figure 2b, inset), which indicates the existence of magnetic ordering in the sample.

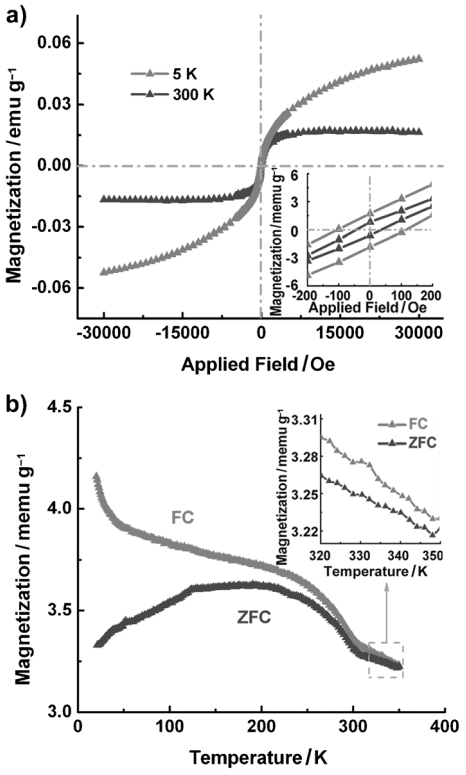

Figure 2. Magnetic properties of nanostructured Bi_2Te_3 HAs. a) Representative hysteresis loop of caterpillar-like Bi_2Te_3 HAs at 5 and 300 K, respectively. b) Temperature-dependent magnetizations (FC and ZFC) of caterpillar-like Bi_2Te_3 HAs under an applied field of 500 Oe. Insets show the high-magnification profiles of corresponding intersections for (a) and (b).

Furthermore, we have performed magnetic measurements on commercial bulk Bi_2Te_3 (Figure S5) and confirmed the diamagnetic nature of the bulk material, which is in agreement with previous reports.[7] We have also ruled out the existence of ferromagnetic impurities in the synthesized Bi_2Te_3 HAs samples. The inductively coupled plasma optical emission spectroscopy (ICP-OES) was carried out on trace metals in the as-prepared Bi_2Te_3 HAs products (Table S1). It was found that the HAs samples possess a Bi-rich composition with negligible ferromagnetic impurities (including, Cr, Mn, Fe, Co, and Ni in the ppm range) which are irrelevant to the observed magnetization. More importantly, the precursors of both $Bi(Ac)_3$ (Ac = acetate) and Te powders were measured to be nonmagnetic and contain similar quantities of the ferromagnetic impurities to those of the as-prepared Bi_2Te_3 HAs products (Figure S5 and Table S2). Therefore, we can safely conclude that the observed magnetism in nanostructured Bi_2Te_3 is robust and intrinsic. We also performed the magnetic response of several samples with various stoichiometries obtained at the different ripening temperatures, as shown in Figure S7. Therein, the stoichiometric ratios of Bi/Te are determined by the ICP-OES measurements, further indicating a Bi-rich nature. As the temperature increases, the amount of Bi relative to Te decreases, accompanied by a decrease in the magnetic moment from 0.053 to 0.017 emu g^{-1}.

To shed light on the origin of the ferromagnetism in nanostructured Bi_2Te_3 HAs, a $2 \times 2 \times 1$ supercell model was constructed (Figure 3a). In this model, each charge-neutral layer consists of five covalently bonded atomic planes ordered in a Te1-Bi-Te2-Bi-Te1 sequence along the c axis; this is known as a quintuple layer (QL). Therein, Te has two different coordination environments: Te1 is bonded to three Bi atoms in the QL and interacts with three Te1 atoms in the adjacent QL by van der Waals forces. The Te2 atom, playing the role of an inversion center, is octahedrally coordinated

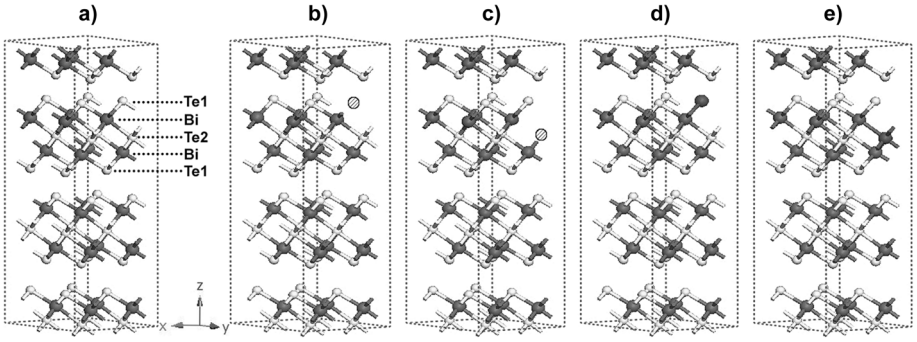

Figure 3. The model configurations of the Bi_2Te_3 supercell, with and without defects. a) Perfect hexagonal $2\times2\times1$ Bi_2Te_3 supercell with quintuple layers with a sequence of Te1-Bi-Te2-Bi-Te1 along the *c* axis. b) A Te1 vacancy created by removing one Te1 atom, denoted as V_{Te1}. c) A Te2 vacancy from the removal of one Te2 atom, denoted as V_{Te2}. d) A Te1 antisite defect (one Te1 atom replaced by one Bi atom), denoted as Bi_{Te1}. e) A Te2 antisite defect (one Te2 atom replaced by a Bi atom), denoted as Bi_{Te2}. The white and gray spheres represent Te and Bi atoms, respectively, whereas the striated sphere shows the site where the atom was removed to generate a Te vacancy.

with six Bi atoms. The Bi atom is bonded to three Te1 atoms and three Te2 atoms. According to the experimental observation of an excessive amount of Bi, we mainly consider four most plausible Bi-rich cases (Figure 3b–e): 1) a Te1 vacancy created by removing one Te1 atom, denoted as V_{Te1}; 2) a Te2 vacancy from the removal of one Te2 atom, denoted as V_{Te2}; 3) a Te1 antisite defect by replacing one Te1 atom with one Bi atom, denoted as Bi_{Te1}; 4) a Te2 antisite defect by replacing one Te2 atom with one Bi atom, denoted as Bi_{Te2}. The lattice parameters and internal coordinates of all structures were fully relaxed after the creation of vacancies or substitutional defects.

The spin-polarized calculations were performed, and the results are shown in Figure 4. It can be clearly seen that both the spin-up and spin-down channels share symmetric distributions for the cases of V_{Te1}, V_{Te2}, and Bi_{Te1} (Figure 4a–c). Whereas, in the case of Bi_{Te2}, an asymmetric density of states (DOSs) for spin-up and spin-down channels (highlighted by the asterisks and frame in Figure 4d) is evident, creating ferromagnetism within the Bi_{Te2}-defective model. Our calculations further show that the Bi_{Te2} supercell carries a total magnetic moment of 0.572 μ_B, where the contribution to the magnetism largely comes from the guest Bi atom. This Bi atom possesses a local magnetic moment of 0.175 μ_B, which mainly originates from the *p* orbit (0.173 μ_B), as shown in Table S3. The theoretical calculation values agree well with the experimental results, and are on the same order of magnitude (see the Supporting Information for details). Furthermore, the partial DOSs of Bi and Te atoms in the Bi_{Te2}-supercell are plotted in Figure S8. It demonstrates that all of the atoms make a contribution to the total magnetic moment, the majority of which are derived from the *p* orbits of the atoms. Our calculations have thus rationalized the experimental observation of magnetism in Bi_2Te_3 HAs towards the point defect of Bi_{Te2}.

Particularly, the intrinsic RTFM behavior of dopant-free thin films or nanoscale materials is of great interest[8] although the origin of magnetism remains in dispute. Given the nonmagnetic nature of HfO_2, the discovery of ferromagnetic order in thin films comes as a surprise.[9] Theoretical calculations suggested that the ferromagnetism in HfO_2 is related to the cation vacancy.[10] Meanwhile, similar ferromagnetism was reported in other nonmagnetic materials such as CaB_6 or CaO, for which point defects of B_6 and Ca vacancies are believed to be responsible for the observed ferromagnetism.[8a,b] Recently, Xu et al. have demonstrated that a magnetic moment can be introduced into nominally nonmagnetic ZnS nanowire at room temperature, owing to the presence of a Zn vacancy.[8c] In our study, the most striking result is the observation of RTFM behaviors in nanostructured Bi_2Te_3 HAs that does not appear in its bulk counterpart. First-principles computations reveal that the magnetic moment is induced by the antisite

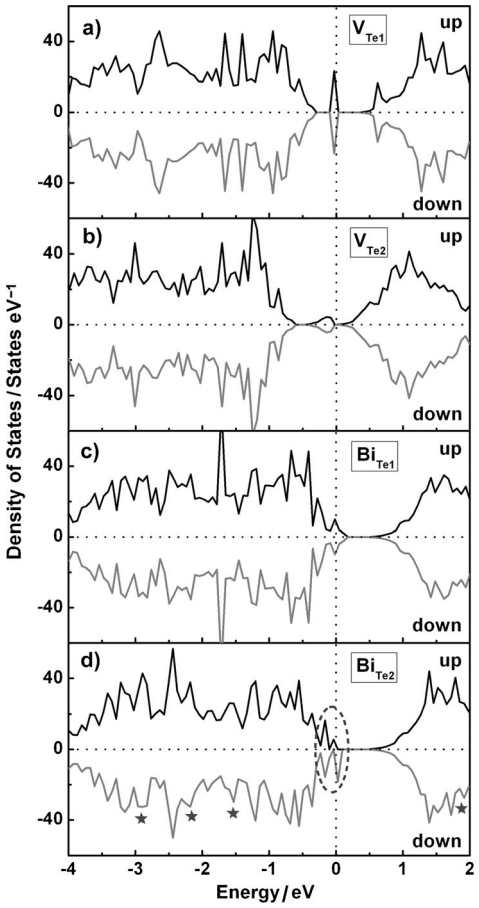

Figure 4. Spin-resolved total density of states (DOSs) of four defective Bi_2Te_3 cases. Spin-resolved total DOSs of a Te1 vacancy (a), a Te2 vacancy (b), a Te1 antisite defect (c), and a Te2 antisite defect (d). The asterisks and frame show the asymmetric features of DOSs for spin-up and spin-down channels. The vertical dashed line indicates the position of the Fermi level ($E_F = 0$ eV).

substitution of Bi for Te. Such a mechanism is essentially different from those of vacancy-defect-induced ferromagnetism, thus providing new insights into the origins of magnetism. Furthermore, introducing magnetic order into topological insulators would lift the time-reversal symmetry protection of the Dirac point, thereby resulting in an energy gap that separates the upper and lower branches of the Dirac cone.[11] Opening up of the Dirac point can thus occur on the surface of such prepared Bi_2Te_3 HAs with intrinsic RTFM, which is a prerequisite for achieving the QAH effect.

In summary, we have observed intriguing RTFM behavior in caterpillar-like Bi_2Te_3 HAs prepared through a facile solution-based route. First-principles calculations indicate that the intrinsic point defect with regard to Bi_{Te2} gives rise to a ferromagnetic order at room temperature, even in the absence of magnetic impurities. Our present work offers an opportunity to promote the further development of low-power-consumption electronics and topological quantum computing.

Experimental Section

Chemicals: Bismuth(III) acetate ($Bi(Ac)_3$, $\geq 99.99\,\%$), oleic acid (OA, 90 %), 1-octadecene (ODE, 90 %) and trioctylphosphine (TOP, 90 %) were purchased from Aldrich. Commercial bulk bismuth telluride (Bi_2Te_3, 99.98 %) was obtained from Alfa Aesar. Tellurium powder (Te, 5N) was received from Sinopharm Chemical Reagent Co. Ltd. Commercially available, analytical-grade toluene, methanol, chloroform, and acetone were used. All chemicals were used without further purification.

Synthesis of caterpillar-like Bi_2Te_3 hierarchical architectures: All experiments were carried out through standard airless techniques: a vacuum/dry nitrogen Schlenk line was used for the synthesis, and a nitrogen glove box for storing and handling air- and moisture-sensitive chemicals. The TOPTe solution was prepared in a Schlenk line by dissolving elemental tellurium in TOP at 250 °C for 4 h. We employed $Bi(Ac)_3$ and TOPTe as starting materials in the presence of OA and ODE as ligand and solvent, respectively. In a typical synthetic procedure, in a glove box, $Bi(Ac)_3$ (0.2 mmol), OA (1 mL) and ODE (6 mL) were loaded into a 50 mL three-neck flask equipped with rubber septum. Then the flask was sealed and taken out and connected to a Schlenk line fitted with a condenser. The mixture was heated to 130 °C and degassed for 20 min to form a colorless solution and the moisture was removed under a nitrogen flow and vigorous magnetic stirring. Then the colorless solution was allowed to cool down naturally to room temperature. Thereafter, the premade TOPTe (1.5 mL) was added into the $Bi(Ac)_3$ solution and stirring maintained for another 5 min. Finally, the mixed solution was transferred to Teflon-lined autoclaves (at up to 80 % capacity) and sealed. Subsequently, the autoclaves were heated to 200 °C for 4 h and then allowed to cool naturally to room temperature. The black precipitate was purified with toluene and methanol, and then a small amount of chloroform and an excess of acetone were added for two more washings.

Computation: First-principles density functional theory (DFT) computations were performed using the plane-wave pseudopotentials technique with generalized gradient approximation (GGA),[12] as implemented in the Vienna ab initio simulation package (VASP).[13] Bi_2Te_3 has a tetradymite crystal structure with the space group $R\bar{3}m$. We considered a hexagonal $2\times2\times1$ Bi_2Te_3 supercell model consisting of 60 atoms in our calculations. A plane–wave basis set with an energy cutoff of 400 eV was used, and the Brillouin zone sampling for geometry optimizations was performed using a $4\times4\times1$ Monkhorst-Pack k-points mesh. The convergence thresholds were set at values of 10^{-5} eV for energy and 10^{-2} eV Å^{-1} for force, respectively.

Characterization: An X-ray powder diffractometer (Shimadzu, XRD-6000) manipulated at 40 kV and 40 mA with Cu Kα radiation ($\lambda = 1.5406$ Å) was used to record the X-ray diffraction (XRD) patterns of the samples. The field-emission scanning electron microscopy (FESEM) measurements were carried out with a scanning electron microscope (JEOL, JSM-6700F) operated at an acceleration voltage of 8 kV. The composition of the specimens was analyzed with an energy-dispersive X-ray (EDX) spectroscopy (INCA energy) attached to the JSM-6700F. Transmission electron microscopy (TEM) and high-resolution transmission electron microscopy (HRTEM) images were obtained on a JEM-2200FS with an emission gun operating at 200 kV. Magnetic property measurements were conducted on a Quantum Design MPMS superconducting quantum interference device (SQUID) VSM magnetometer. Samples with a weight of 6.3 mg were fixed in nonmagnetic gelatin capsule holders. Any possibly undesired signals caused by the instrument or sample holders have been automatically deducted during the testing process as background. Furthermore, the spatula was cleaned before being used to transfer the powder to avoid the introduction of any magnetic impurities. Inductively coupled plasma-optical emission spectroscopy was performed with a PerkinElmer OPTIMA 3300 DV analyzer. The electron spin resonance (ESR) spectroscopy was obtained on a JES-FA 200 ESR spectrometer. The instrumental parameters were as follows: scanning frequency, 9.45 GHz; central field, 4000 Gs; scanning width, 8000 Gs; scanning power, 0.998 mW; scanning temperature, 25 °C. X-ray photoelectron spectroscopy (XPS) was investigated by a VG ESCALAB MKII spectrometer with a Mg KR excitation (1253.6 eV).

Received: October 29, 2013
Published online: December 4, 2013

Keywords: ab initio calculations · ferromagnetism · Hall effect · nanostructures · topological insulators

[1] a) A. Majumdar, *Science* **2004**, *303*, 777–778; b) L. Zhu, H. Wang, Y. Wang, J. Lv, Y. Ma, Q. Cui, Y. Ma, G. Zou, *Phys. Rev. Lett.* **2011**, *106*, 145501; c) J. L. Zhang, S. J. Zhang, H. M. Weng, W. Zhang, L. X. Yang, Q. Q. Liu, S. M. Feng, X. C. Wang, R. C. Yu, L. Z. Cao, L. Wang, W. G. Yang, H. Z. Liu, W. Y. Zhao, S. C. Zhang, X. Dai, Z. Fang, C. Q. Jin, *Proc. Natl. Acad. Sci. USA* **2011**, *108*, 24–28.

[2] a) H. B. Zhang, H. L. Yu, D. H. Bao, S. W. Li, C. X. Wang, G. W. Yang, *Adv. Mater.* **2012**, *24*, 132–136; b) H. B. Zhang, H. L. Yu, D. H. Bao, S. W. Li, C. X. Wang, G. W. Yang, *Phys. Rev. B* **2012**, *86*, 075102.

[3] a) H. Zhang, C. X. Liu, X. L. Qi, X. Dai, Z. Fang, S. C. Zhang, *Nat. Phys.* **2009**, *5*, 438–442; b) Y. L. Chen, J. G. Analytis, J.-H. Chu, Z. K. Liu, S.-K. Mo, X. L. Qi, H. J. Zhang, D. H. Lu, X. Dai, Z. Fang, S. C. Zhang, I. R. Fisher, Z. Hussain, Z.-X. Shen, *Science* **2009**, *325*, 178–181; c) J. Zhang, C.-Z. Chang, Z. Zhang, J. Wen, X. Feng, K. Li, M. Liu, K. He, L. Wang, X. Chen, Q.-K. Xue, X. Ma, Y. Wang, *Nat. Commun.* **2011**, *2*, 574; d) T. Arakane, T. Sato, S. Souma, K. Kosaka, K. Nakayama, M. Komatsu, T. Takahashi, Z. Ren, K. Segawa, Y. Ando, *Nat. Commun.* **2012**, *3*, 636.

[4] a) R. Yu, W. Zhang, H.-J. Zhang, S.-C. Zhang, X. Dai, Z. Fang, *Science* **2010**, *329*, 61–64; b) C.-Z. Chang, J. Zhang, X. Feng, J. Shen, Z. Zhang, M. Guo, K. Li, Y. Ou, P. Wei, L.-L. Wang, Z.-Q. Ji, Y. Feng, S. Ji, X. Chen, J. Jia, X. Dai, Z. Fang, S.-C. Zhang, K. He, Y. Wang, L. Lu, X.-C. Ma, Q.-K. Xue, *Science* **2013**, *340*, 167–170.

[5] a) L. Fu, C. L. Kane, *Phys. Rev. Lett.* **2009**, *102*, 216403; b) X.-L. Qi, R. Li, J. Zang, S.-C. Zhang, *Science* **2009**, *323*, 1184–1187.

[6] a) L.-Q. Mai, F. Yang, Y.-L. Zhao, X. Xu, L. Xu, Y.-Z. Luo, *Nat. Commun.* **2011**, *2*, 381; b) G. Xiao, Q. Dong, Y. Wang, Y. Sui, J. Ning, Z. Liu, W. Tian, B. Liu, G. Zou, B. Zou, *RSC Adv.* **2012**, *2*, 234 – 240.
[7] M. Z. Hasan, J. E. Moore, *Annu. Rev. Condens. Matter Phys.* **2011**, *2*, 55 – 78.
[8] a) I. S. Elfimov, S. Yunoki, G. A. Sawatzky, *Phys. Rev. Lett.* **2002**, *89*, 216403; b) R. Monnier, B. Delley, *Phys. Rev. Lett.* **2001**, *87*, 157204; c) G. Zhu, S. Zhang, Z. Xu, J. Ma, X. Shen, *J. Am. Chem. Soc.* **2011**, *133*, 15605 – 15612; d) J.-I. Hong, J. Choi, S. S. Jang, J. Gu, Y. Chang, G. Wortman, R. L. Snyder, Z. L. Wang, *Nano Lett.* **2012**, *12*, 576 – 581.
[9] M. Venkatesan, C. B. Fitzgerald, J. M. D. Coey, *Nature* **2004**, *430*, 630 – 630.
[10] C. Das Pemmaraju, S. Sanvito, *Phys. Rev. Lett.* **2005**, *94*, 217205.
[11] a) Q. Liu, C.-X. Liu, C. Xu, X.-L. Qi, S.-C. Zhang, *Phys. Rev. Lett.* **2009**, *102*, 156603; b) Y. Chen, J. H. Chu, J. Analytis, Z. Liu, K. Igarashi, H. H. Kuo, X. Qi, S. K. Mo, R. Moore, D. Lu, *Science* **2010**, *329*, 659 – 662; c) K. Nomura, N. Nagaosa, *Phys. Rev. Lett.* **2011**, *106*, 166802; d) C.-X. Liu, X.-L. Qi, X. Dai, Z. Fang, S.-C. Zhang, *Phys. Rev. Lett.* **2008**, *101*, 146802.
[12] J. P. Perdew, K. Burke, M. Ernzerhof, *Phys. Rev. Lett.* **1996**, *77*, 3865 – 3868.
[13] G. Kresse, J. Furthmüller, *Phys. Rev. B* **1996**, *54*, 11169 – 11186.

